Study on the impact of Pr^{3+}, Ce^{3+}, and Pb^{2+} ions on luminescence properties of $BaB_8O_{13}:Gd^{3+}$ for potential applications in phototherapy

MLA Letswalo*, SB Sebopa and BM Sondezi

Department of Physics, University of Johannesburg, 55 Beit St, Doornfontein, Johannesburg, 2028, South Africa.

E-mail: letswalom@uj.ac.za

Abstract. A series of BaB_8O_{13} phosphors doped with different concentrations of 2 mol.% Gd^{3+} ions and 1.0 mol.% co-doped with Pr^{3+}, Pb^{2+} and Ce^{3+} ions were synthesized by the combustion synthesis method. The X-ray powder diffraction (XRD) analysis confirmed the pristine crystalline structure and uniformity of the compounds, with an average crystalline size of around 33 – 45 nm. Scanning Electron Microscopy (SEM) was performed to study the surface morphology of the compound, and the bandgap was influenced by the incorporation of 2 mol.% Gd^{3+} ions and 1.0 mol.% co-doped with Pr^{3+}, Pb^{2+} and Ce^{3+} as confirmed from the diffuse reflectance. data. The photoluminescence (PL) excitation spectra of $BaB_8O_{13}:Gd^{3+}$ phosphor showed excitation peaks at 274 nm. The crucial role of gadolinium (Gd^{3+}) ions in barium-based hosts lies in their narrow-band emission spectrum, specifically at 311 – 315 nm, which is in the narrow band ultraviolet B (NB- UVB) range and is attributed to the $^6P_{7/2}$ to $^8S_{7/2}$ transition and a prominent emission peak at around 347 nm that could result from oxygen vacancy in the BaB_8O_{13} compound. The effects of co-doping sanitizers to Gd^{3+} ions on PL emission at 311 nm were as follows: $Ce^{3+} > Pr^{3+}$, $> Pb^{2+}$. Through effective energy transfers from the sensitizers, the broad emission at 387 nm was suppressed while the PL emission of the Gd^{3+} ion at 311 nm was increased. BaB_8O_{13}:2%Gd^{3+} co-doped with 1 mol% Ce^{3+} dominating. Through phototherapy, such material-enhanced NB-UVB emission may be used as a viable treatment option for a variety of skin conditions, including vitiligo, eczema, and psoriasis.

1. Introduction

Natural sunlight, also known as heliotherapy, was used in ancient times to treat a variety of skin diseases successfully [1]. Nowadays, artificial light, known as phototherapy, is used effectively to treat a whole array of skin diseases with heightened success. Phototherapy is the interaction of light of specific wavelengths on tissues of the skin to inflict a change in its immune response system with reduced erythemal side effects [2]. Light-emitting devices with a phosphor-based coating encapsulated on the inner side of the lamp, and with a wavelength of light emission that aligns with the action spectrum of the skin disease, can be used effectively in this case [3]. Phosphor materials that absorb strongly in the UVC region [200 -280 nm] and for emissions in the narrow-band NB-UVB region [311 – 315 nm] are good for the treatment of skin diseases such as psoriasis as it aligns to the action spectrum of the disease. Minimal literature points towards light emissions in the UVA region [320 - 400 nm], which is useful for a broader treatment of other skin diseases. A typical phosphor material is host dependent and, in this regard, barium octa borate BaB_8O_{13} has been chosen as a host because it has high thermal and chemical stability, it has superior optical properties and has strong absorption the UVC region [4]. Additionally, an ideal dopant such as gadolinium ion (Gd^{3+}), a rare earth ion whose emission was found to be aligned to a NB-UVB region that is attributed to $^6P7_{/2}$ to $^8S_{7/2}$ transition for wavelength excitation of 274 nm. In general, these 4*f* -4*f* transitions in Gd^{3+} ions are weak, sensitizers such as Bi^{3+}, Ce^{3+}, Pr^{3+} and Pb^{2+} are

incorporated to enhance its emission in the NB-UVB region by these ions effectively absorbing the excitation energy and transferring it non-radiatively to the Gd^{3+} activator ion.
In this work, BaB_8O_{13} is synthesized by a high temperature solid-state reaction synthesis method. BaB_8O_{13} is doped with Gd^{3+} and co-doped with Pr^{3+}, Ce^{3+} and Pb^{2+} ions. The structural, morphological and optical properties, determined by X-ray diffraction (XRD), Scanning electron microscopy (SEM) and UV-visible techniques, respectively. The luminescence properties of these phosphor materials are studies using the photoluminescence (PL) techniques.

2. Experimental

Material and synthesis techniques

Barium octaborate BaB_8O_{13} doped with Gd^{3+} ions was synthesized by the combustion synthesis method. In preparation of this compound, barium nitrate ($Ba(N_2O)$, boric acid H_3BO_3 and urea (CH_4N_2O) was used as raw materials. Stoichiometric proportions of the precursor's materials were weighted and mixed in distilled water and ground in a mortar and pestle until a homogeneous solution produced. To ensure better homogeneity of the solution, the mixture was then transferred to a crucible and thereafter transferred to the furnace for annealing at a constant temperature of 800 ^oC for approximately 4 hours. Once the furnace was cooled to room temperature, the mixture was again ground and was made ready for characterization.

3. Material characterization Techniques

X-ray diffraction of the prepared samples was measured using a PANanalytical X'pert powder diffractometer having a wavelength of 1.5406 Å for a CuK_α line radiation. SEM measurements were done to determine the surface morphology, and the particle sizes of the prepared materials was obtained using a JSM – 2100 microscope operating at 20 kV voltage. Energy dispersive spectroscopy (EDS) at specific points on the sample were done to obtain the elemental composition of the prepared materials. UV-vis spectroscopy was performed to measure the sample's absorbance or transmittance, done within a spectral range of 200 – 800 nm. Optical measurements were done using a photoluminescent spectrometer, employing a Horiba QN8000 instrument, encased with a xenon lamp as a light source, and a PPD- 850 detector with a fluorescence spectrophotometer with s spectral measuring range of 200 – 600 nm.

4. Results and Discussions

Structural Investigations

Figure 1 shows the X-ray diffraction patterns of the BaB_8O_{13}, Gd^{3+} (2 mol%) doped BaB_8O_{13}, co-doped with a fixed 1 mol% of Ce^{3+}, Pr^{3+}, and Pb^{2+} ions, in the range of 10° to 50°. XRD patterns show an orthorhombic crystal structure formation with lattice parameters of a = 13.2Å, b = 17.38Å and c = 8.56Å [5] having a space group of $P4_122$. These patterns are well compatible with the reference patterns from the JCPDS file #00-006-0277, as indicated in the Figure 1. This pristine orthorhombic structure is seen to have no impurity peaks, confirming a successful incorporation of Gd and co-doped Pr, Ce, and Pb ions. The average crystalline size, determined using the Scherrer equation, was 36.69 nm for the host material. It increased slightly to 37.05 nm with Gd^{3+} doping, but decreased to 35.75 nm with Pr^{3+}, 35.97 nm with Ce^{3+}, and 35.82 nm with co-doping. When a small Gd^{3+} ion (r = 1.05 Å) substitutes for a larger Ba^{2+} ion (r = 1.35 Å) in the host lattice, it causes a decrease in the Gd^{3+}– O^{2-} bond distance, which leads to an increase in the crystal field splitting and a shift in the peak positions [3].

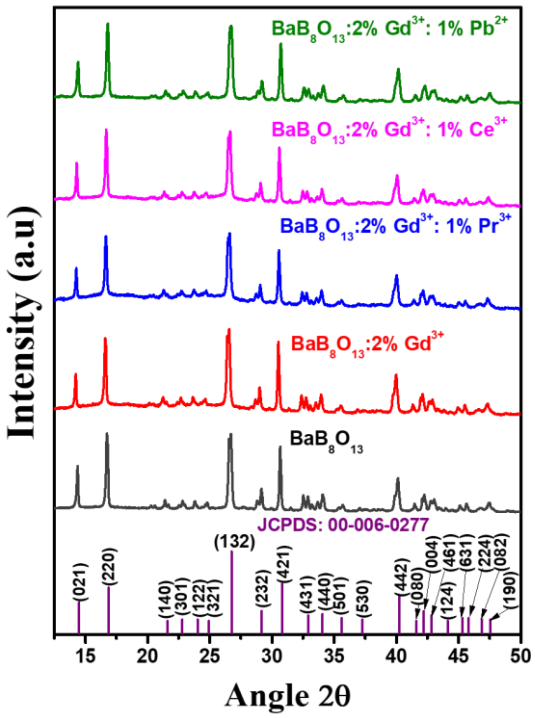

Figure 1. XRD patterns of BaB_8O_{13}, 2 mol% Gd^{3+}-doped BaB_8O_{13}, and co-doped with a fixed 1 mol% of Ce^{3+}, Pr^{3+}, and Pb^{2+} ions.

Morphological Investigations

Figure 2 shows the SEM images of the BaB_8O_{13}, BaB_8O_{13}:2%Gd3+and co-doped BaB_8O_{13}:2%Gd^{3+} material. SEM images reveal the formation of a pristine crystalline material with uniform crystal structure. Further, it is revealed that the synthesized particles are inhomogeneous, clustered closely and evolve in size and shape when doped with 2 mol% Gd^{3+} or co-doped with Ce^{3+}, Pr^{3+} or Pb^{2+} ions as shown in Figure 2 (a-e). In general, the topology and morphology of the prepared samples change with doping and co-doping. EDS spectra of compounds show the main elements such as Barium, Boron and Oxygen. Carbon and Iridium (Ir) probably came from the carbon tape mountings and coating layers (used to prevent charging), respectively, in Figure 2 (a-e). Moreover, the selected chemical image mapping image scans describe the uniform distribution of these elements throughout the materials, as depicted in Figure 2 (f).

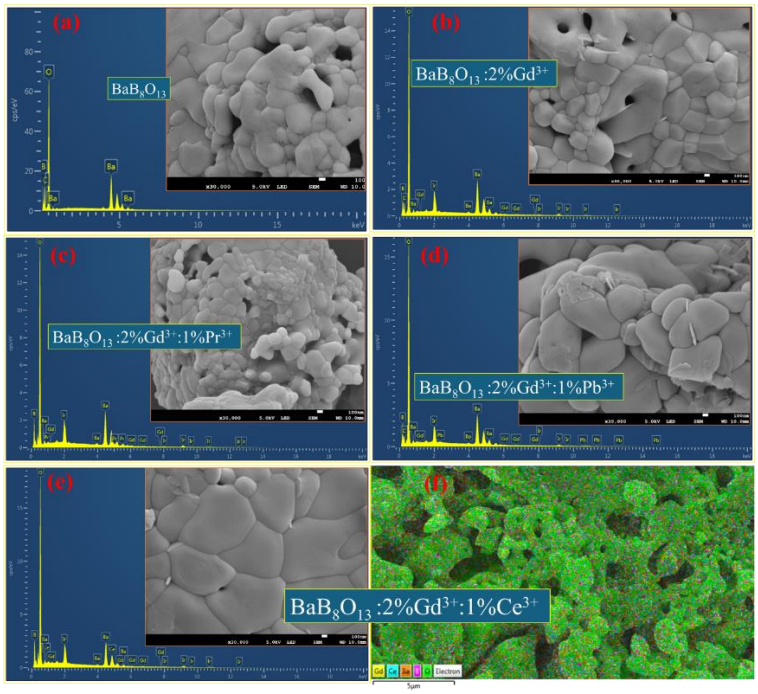

Figure 2. SEM images and respective EDS of the host material BaB_8O_{13} in (a) Gd^{3+}-Gd^{3}-doped (2 mol% fixed) in (b), 1 mol% Pr^{3+} co-doped in (c), 1 mol% Pb^{2+} co-doped in (d), and 1 mol% Ce^{3+} co-doped in (e) and mapping spectra of 1 mol% Ce^{3+} co-doped in (f).

Optical Investigations

UV-vis diffuse reflectance spectra of the doped and co-doped materials in the wavelength range from 200 to 800 nm were measured, as shown in Figure 3 (a). In the case of the host material, we observe high absorption, making it an ideal candidate for luminescence. Remarkable absorptions are observed for the doped and co-doped samples at their respective absorption edges: around 250 nm for the co-doped samples containing 1 mol% Pb^{2+} and 1 mol% Pr^{3+} ions, while the redshifted samples doped with 2 mol% Gd^{3+} and co-doped with 1 mol% Ce^{3+} exhibit absorption edges at approximately 450 nm and 750 nm, respectively. The band gap of these samples is estimated using the Kubelka-Munk absorption coefficient (K/S), given by: $F(R) = K/S = (1-R)^2/2R$, where R is the reflectivity, K is the absorption coefficient and S is the scattering coefficient [6,7]. The band gap of the samples is obtained by extrapolating the linear section of the Tauc plots, as shown in Figure 3(b). The optical band gap of these samples ranges from 3.13 eV to 5.39 eV.

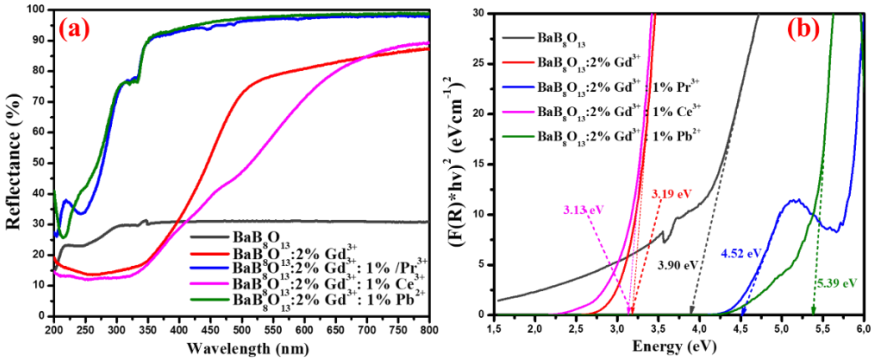

Figure 3(a): Reflectance spectra of 2 mol% Gd^{3+}-doped BaB_8O_{13} host material, co-doped with a fixed 1 mol% of Ce^{3+}, Pr^{3+}, and Pb^{2+} ions, while **Figure 3(b)** shows the Tauc plots of the same prepared samples.

The PLE excitation spectra of the BaB_8O_{13} host material, measured at an emission wavelength of 311 nm, is shown in the insert of Figure 4 (a), while its PL spectra is shown in Figure 4(a) The PLE spectra

of host shows a broad spectrum in the UVC region with a maximum at 274 nm, attributed to $^8S_{7/2}$ to ^6I_J transition, corresponding to 4*f* to 5*d* orbital transition and a charge transfer from O^{2-} (2p orbital) to Gd^{3+} (4*f* orbital) [3]. Figure 4(b) shows the PL emission spectra of Gd^{3+}-doped BaB_8O_{13} co-doped with 1 mol% of Ce^{3+}, Pr^{3+}, and Pb^{2+} ions, recorded under an excitation wavelength of 274 nm. The PL spectrum shows a sharp NB-UVB emission at 311 nm due to $^8P_{7/2}$ to $^8S_{7/2}$ transition, followed by a broadband emission centred around 387 nm for all samples except for co-doped 1 mol% Ce^{3+} which has a maximum around 350 nm. In addition, we observe that the broad emission for the host at 347 nm is red-shifted as the sensitizers are incorporated to around 350-387 nm. It is observed that after doping BaB_8O_{13} with 2 mol% Gd^{3+} and co-doping it with 1 mol% Ce^{3+} and 1% mol Pr^{3+}, the broadband emissions appear to be suppressed, allowing for the Gd^{3+} emission at 311 nm to be enhanced, suggesting that whilst the broadband emissions are reduced then the PL emission of Gd^{3+} is enhanced. It is further noticed that the emissions at 516, 599, and 645 nm are attributed to Pb^{2+} emission ions is attributed to the transition of the Pb^{2+} ($sp\text{-}s^2$) related charge-transfer state. [8]. Additionally, emissions in the visible regions are also observed for these samples, which makes these samples also applicable for LEDs. The broadband emission is attributed to oxygen vacancies (or oxygen interstitials) and surface defects [9]. when Ce^{3+} is co-doped with 2 mol% Gd^{3+}, it has a lower band gap energy which accounts for its enhanced emissions at 311 nm compared to the other co-dopants. In this respect, the 2 mol% Gd^{3+} doped BaB_8O_{13} and co-doped with 1 mol% Ce^{3+} has the strongest emission in the NB-UVB region at 311 nm, while the compound co-doped with Pb^{2+} and single doped 2%Gd^{3+} ions has the strongest emission in the broadband region. These compounds, used in tandem as a coating in phosphor lamps, could treat a myriad of skin diseases, instead of psoriasis, as in conventional skin treatments.

Energy transfer mechanisms

Figure 5 shows the schematic model of the possible energy transfers from the sensitizers (Ce^{3+}, Pr^{3+} and Pb^{2+}) ions to the activator Gd^{3+} ion in the doped BaB_8O_{13} phosphor material. An observation of the PL spectra in Figure 4, it is observed that enhanced emissions at 311 nm is obtained for the 1 mol% Ce^{3+} co-doped BaB_8O_{13}:2%Gd^{3+} phosphor, implying efficient energy transfers occurs mainly from Ce^{3+} to Gd^{3+} when equilibrium was established between their excited states. Additionally, some energy transfers of a moderate intensity do occur from Pr^{3+} to Gd^{3+} ion at 311 nm. Furthermore, low intensity energy transfer does occur from Pb^{2+} to Gd^{3+} ions at 311 nm.

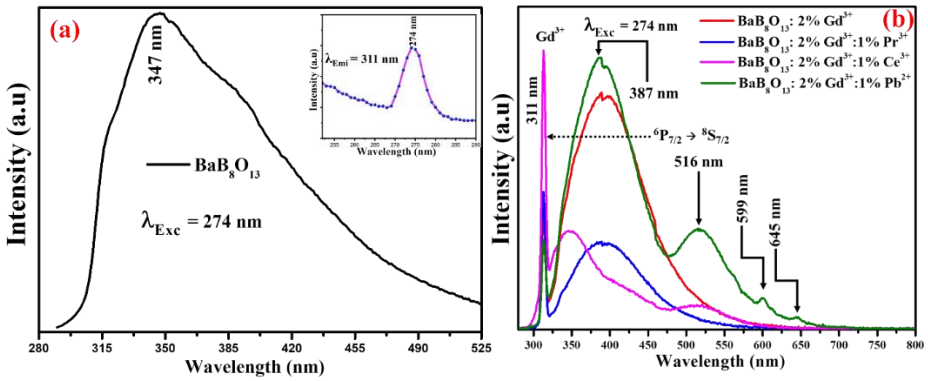

Figure 4(a): Shows the PL spectra of the host, while insert shows its PLE spectra and **Figure 4(b)** shows the PL spectra of doped and co-doped samples.

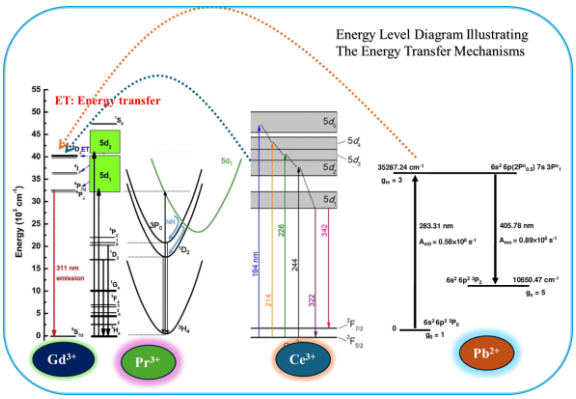

Figure 5: Possible schematic model of the energy transfers from the sensitizers (Ce^{3+}, Pr^{3+} and Pb^{2+}) to the Gd^{3+} activator ions in the BaB_8O_{13} host material [10, 11].

5. Conclusion

Gd^{3+} doped BaB_8O_{13} and co-doped materials with sensitizers (Ce^{3+}, Pr^{3+} and Pb^{2+}) show NB-UV-B, UV-A and visible emissions when synthesized by the combustion method at 800 ^{0}C. The PL spectra show that the UV-B emissions fall in the 311 nm region when excited by a wavelength of 274 nm. The sharp UV-B emissions at 311 nm corresponds to $^6P_{7/2}$ to $^8S_{7/2}$ transition from its metastable state to its ground state, and abroad band emission at around 375 nm due to oxygen defect related sources. The XRD data for the BaB_8O_{13} material conforms with JCPDS data having an orthorhombic structure. The SEM results confirm the presence of elements existing in the Gd^{3+} doped BaB_8O_{13} materials. UV-vis measurements indicates that these materials are good for luminescence studies due to their strong absorptions in the UV region. The energy transfer between Ce^{3+} and Gd^{3+} ions makes this compound $BaB_8O_{13}:Ce^{3+}/Gd^{3+}$ an ideal candidate for applications in phototherapy lamps, followed by $BaB_8O_{13}:Pr^{3+}/Gd^{3+}$ and $BaB_8O_{13}:Pb^{2+}/Gd^{3+}$ encapsulated lamps in that order. The broadband emissions of the $BaB_8O_{13}:Pb^{2+}/Gd^{3+}$ and $BaB_8O_{13}:Gd^{3+}$ compounds together with the strong NB-UVB emission of $BaB_8O_{13}:Ce^{3+}/Gd^{3+}$ makes them ideal for treating a multitude of skin diseases. Furthermore, emission is also observed in the visible region, thus allowing them to operate in LED lights as well.

6. References

[1] Bawanthade BP, Mistry AA, Ugemuge N, Chaudari IS and Dhoble SJ, *Luminescence* 2024 **39** e4736.

[2] Krutmann J, Morita A. 1999 *Journal of Investigative Dermatology Symposium Proceedings* **4(1)** 70.

[3] Sharma AA, Rakshita, Pradhan PP, Durga Prasad KAK, Mishra S, Jayanthi K and Haranath D 2023 *Journal of Material Research* **38** 2812.

[4] Lanje MM, Yawalkar MM, Dahegaonkar JS and Dhoble SJ 2021 International Conference on Research Frontiers in Sciences *Journal of Physics: Conference Series* **1913** 012031.

[5] Erdogomus E, Orkmaz E and Kafadar VE 2014 *J Appl. Spectrosc*. **80** 952.

[6] Yu H, Deng D, Hua Y, Li C and Xu S 2014 Rsc. Adv. **6** 82824.

[7] Gupta P, Bedyal AK, Kumar V, Khajuria Y, Sharma V, Ntwaeaborwa OM and Swart HC 2015 *Mater. Res. Express* **2** 076202.

[8] Kuang, J. and Liu, Y. (2006) 'Luminescence properties of a Pb^{2+} activated long-afterglow phosphor', Journal of The Electrochemical Society, 153(3). doi:10.1149/1.2163780.

[9] Lephoto MA, Tshabalala KG, Motloung SJ, Mhlongo GH and Ntwaeaborwa OM 2018 *Journal of Luminescence* **200** 94.

[10] Wu, Y. and Ren, G. (2013) 'Energy transfer and radiative recombination processes in $(Gd,Lu)_3Ga_3Al_2O_{12}:Pr^{3+}$ scintillators', Optical Materials, 35(12), pp. 2146–2154. doi:10.1016/j.optmat.2013.05.039.

[11] Vidal, F. et al. (2008) 'Enhanced laser-induced breakdown spectroscopy by second-pulse selective wavelength excitation', AIP Conference Proceedings, 1047, pp. 25–35. doi:10.1063/1.2999951.